frontiers in Earth Science

ORIGINAL RESEARCH
published: 13 December 2021
doi: 10.3389/feart.2021.766598

Atmospheric CO_2 Consumption by Chemical Weathering in the Main Tributaries of the Yellow River: Tao He, Huang Shui, and Datong He, Originating From the Northeastern Qinghai-Tibet Plateau

Zhuoma Yongji[1,2], *Liuqian Zhao*[1,2], *Yunxiao Li*[3] *and Longjun Zhang*[1,2]*

[1]Key Laboratory of Marine Environmental Science and Ecology, Ministry of Education, College of Environmental Science and Engineering, Ocean University of China, Qingdao, China, [2]Pilot National Laboratory for Marine Science and Technology, Qingdao, China, [3]Environment Science Laboratory, College of Resource and Environment, Shanxi Agricultural University, Taigu, China

OPEN ACCESS

Edited by:
Andrew Jonathan Hodson, The University Centre in Svalbard, Norway

Reviewed by:
Peter Michael Wynn, Lancaster University, United Kingdom
Philip Pogge von Strandmann, University College London, United Kingdom

***Correspondence:**
Longjun Zhang
longjunz@ouc.edu.cn

Specialty section:
This article was submitted to Geochemistry, a section of the journal Frontiers in Earth Science

Received: *29 August 2021*
Accepted: *10 November 2021*
Published: *13 December 2021*

Citation:
Yongji Z, Zhao L, Li Y and Zhang L (2021) Atmospheric CO_2 Consumption by Chemical Weathering in the Main Tributaries of the Yellow River: Tao He, Huang Shui, and Datong He, Originating From the Northeastern Qinghai-Tibet Plateau. Front. Earth Sci. 9:766598. doi: 10.3389/feart.2021.766598

The Tao He, Huang Shui, and Datong He originate from the northeastern margin of the Qinghai-Tibet Plateau (QTP) and flow into the Yellow River on the Loess Plateau (LP), all with a basin area exceeding 15,000 km^2, and are the three largest tributaries of the Yellow River QTP sub-basin. Water samples were collected at the river outlets, the QTP section, the transition zone between the QTP and the LP, and the LP section of each river. These water samples were used to explore CO_2 consumption by chemical weathering and its control mechanisms. Runoff and physical erosion are the main factors controlling chemical weathering in the three rivers. The increase of relief ratio in the transition zone between the QTP and the LP makes the chemical weathering particularly intense in this area. The total CO_2 consumption rates by chemical weathering in the Tao He and Huang Shui transition zones are 1.4 times and 1.7 times greater than in their QTP sections, and 1.7 times and 2.3 times greater than in their LP sections, respectively. In contrast, due to the high relief ratio of 8‰ in the Datong He transition zone, the residence time of the water is extremely short, and unweathered fine-grained materials are delivered downstream to continue weathering. The influence of differential lithology distribution on chemical weathering includes that the Datong He QTP section with carbonate exposure presents the most intense carbonate weathering in that basin, and the Tao He transition zone has low silicate weathering resulting from the distribution of early Permian strata. In addition, groundwater recharge most likely influenced the silicate weathering of Huang Shui significantly. The total area of the three rivers accounts for 25% of the Yellow River QTP sub-basin, while their contribution to the total CO_2 consumption flux by chemical weathering approximates 36%. The silicate weathering of the northern QTP rivers is lower than the global average and significantly lower than those of the southern QTP rivers. However, carbonate weathering of the QTP rivers exhibit no north-south regional differences.

Keywords: Yellow River, Qinghai-Tibet Plateau sub-basin, main tributaries, chemical weathering, CO_2 consumption

1 INTRODUCTION

Chemical weathering of terrestrial rocks regulates global climate by consuming atmospheric CO_2 (Berner et al., 1983), with a global CO_2 consumption by chemical weathering of 0.22–0.29 Gt a^{-1} (Gaillardet et al., 1999; Hartmann et al., 2009). Numerous rivers originate from the Qinghai-Tibet Plateau (QTP), including the Ganges, Brahmaputra, Indus, Yangtze, and Yellow River. Exposure of abundant fresh materials *via* rapid uplift of the QTP produces a relatively high chemical weathering rate here (Raymo and Ruddiman, 1992). Hence, based on the potential influence on the global carbon cycle and climate change, chemical weathering in the QTP, especially net atmospheric CO_2 absorption by silicate weathering on the geological time scales have received considerable attention (Gaillardet et al., 1999; Wu et al., 2005; Wu et al., 2008a, b; Noh et al., 2009). Wu (2016) found that silicate weathering rate is low in the inland rivers on the northern margin of the QTP, and combined with previous studies, suggested that the silicate weathering rate in the QTP may decrease in the order: southern>eastern>western>northern. Subsequently, the study of Jiang et al. (2018) in the small catchments of Mount Gongga on the southeastern QTP and the study of Zhang et al. (2019) in the Yalong River on the eastern QTP show that silicate weathering rates in these basins were lower than those in the rivers on the southern QTP and higher than those in the rivers on the northern QTP. However, due to complex lithologies, multiple climatic and tectonic zones, and increased anthropogenic activities on the QTP, additional information is urgently needed to further understand the spatial variability of chemical weathering and its mechanisms in the QTP.

The Yellow River is one of the main exorheic rivers originating from the QTP. Previous studies attributed a relatively high HCO_3^- concentration in the Yellow River to carbonate weathering within the loess (contains 10–20% carbonate) of the middle Loess Plateau (LP) sub-basin (Zhang et al., 1995; Chen et al., 2005). However, recent studies of the Yellow River have shown that the upper QTP sub-basin has a higher chemical weathering rate compared to the LP sub-basin (Wu et al., 2005; Fan et al., 2014; Wang et al., 2016). Although the QTP sub-basin accounts for only 30% of the Yellow River basin area, the CO_2 consumption flux accounts for 61% of the entire basin's flux (Wang et al., 2016).

The transition zone between the QTP and the LP of the Yellow River often has the highest weathering rate in the basin due to the sharp elevation drop, strong tectonic deformation, and drastic climate change. For example, the highest chemical weathering rate of both the Brahmaputra River (Singh et al., 2005; Hren et al., 2007) and the Yalong River (Zhang et al., 2019) occur in the area with the steepest average slope. Early studies of the Yellow River generally used the Lanzhou Hydrological Station as the boundary between the QTP and the LP (Wu et al., 2005; Fan et al., 2014; Wang et al., 2016). However, two large reservoirs, the Longyangxia and Liujiaxia reservoirs (with storage capacities of 247×10^8 and 57×10^8, respectively), were successively built upstream above the Lanzhou Hydrological Station on the Yellow River mainstream, which flows through the QTP margin (**Figure 1**). The presence of reservoirs alters the seasonal variation of river mass transport and makes it difficult to study the chemical weathering and its mechanism in the transition zone between the QTP and the LP of the Yellow River. The Tao He, Huang Shui, and Datong He (He and Shui mean "river" in Mandarin) are the three largest tributaries of the Yellow River upstream above the Lanzhou station. They originate from the QTP and merge into the Yellow River on the LP. The drainage area of the three rivers is approximately 25% that of the Yellow River QTP sub-basin, and the discharge contributed by these rivers reaches 32% that of the Lanzhou station on the Yellow River mainstream (Wang and Hu, 2011). To date, no medium or larger hydrologic projects have been reported to be in operation in these basins, making this an optimal zone for studying the chemical weathering and its mechanism in the transition zone between the QTP and the LP. However, few studies have focused on chemical weathering in these areas. Most studies have been limited to the ionic composition of downstream water or at the outlets (Wu et al., 2005; Fan et al., 2014; Wang et al., 2016).

The purpose of this paper is to investigate CO_2 consumption by chemical weathering in the QTP sections, the transition zones between the QTP and the LP, and the LP sections of the rivers on the northeastern margin of the QTP (the Tao He, Huang Shui, and Datong He rivers). The study of CO_2 consumption by chemical weathering in the transition zones between the QTP and the LP will help to further understand the chemical weathering mechanism of rivers from orogenic belts such as the QTP. We also present the seasonal variations of CO_2 consumption by chemical weathering in the three rivers. In addition, variations in chemical weathering in different drainage basins on the QTP are compared with rivers in other regions.

2 MATERIALS AND METHODS

2.1 Study Area

The Tao He, Huang Shui, and Datong He are located on the northeast margin of the QTP. The Tao He is located on the southern bank of the Yellow River with a total length of 673 km and a total basin area of 25,527 km^2. The Huang Shui and Datong He are located on the northern bank of the Yellow River and flow eastward, parallel to each other, with the Daban Mountains as a boundary. Their river lengths are 374 and 561 km, and their basin areas are 15,342 and 15,133 km^2, respectively (Wang and Hu, 2011). The QTP sections of the three rivers have an average elevation of about 4,000 m (**Figure 1A**), and an annual temperature of 3.12°C (Yang et al., 2004). There is almost no summer throughout the year, typical of a subalpine semi-arid climate. The outcropping rocks of the Tao He QTP section belong to the Triassic period and mainly contain shales and sandstones (Pang et al., 2018, Gansu Province 1:500,000 geological map, www.ngac.org.cn). The QTP sections of the Huang Shui and Datong He are subject to regional dynamic thermal flow metamorphism of the Qilian fold belt in the Early Mesoproterozoic. In addition to shale, gneiss and schist are

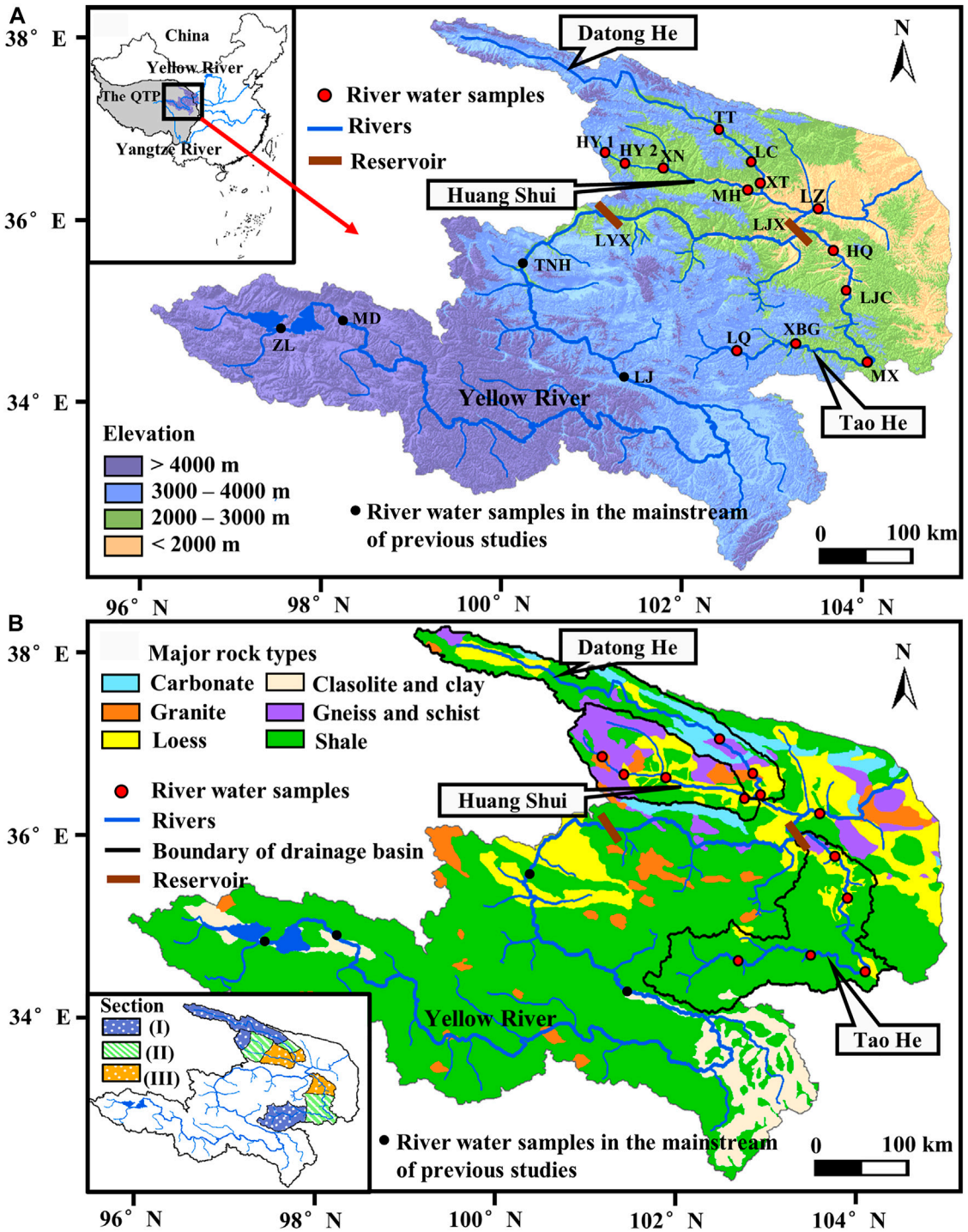

FIGURE 1 | (A) Elevation map and **(B)** Geological map of the Tao He, Huang Shui, Datong He, and Yellow River QTP sub-basin (upstream of the Lanzhou station). Elevation data were taken from https://srtm.csi.cgiar.org/srtmdata/. The geological map is modified from Chen et al. (2005), with reference to Pang et al. (2018) for details. Yellow River: TNH, Tangnaihai; GD, Guide; LZ, Lanzhou; Tao He: LQ, Luqu; XBG, Xiabagou; MX, Minxian; LJC, Lijiacun; HQ, Hongqi; Huang Shui: HY1, Haiyan; HY2, Huangyuan; XN, Xining; MH, Minhe; Datong He: TT, Tiantang; LC, Liancheng; XT, Xiangtang. The inset in panel B shows the study area divided into the (I) QTP sections (the drainage basins upstream Xiabagou of the Tao He, Haiyan of the Huang Shui, and Tiantang of the Datong He), (II) the transition zones between the QTP and the LP (Xiabagou to Lijiacun of the Tao He, Haiyan to Xining of the Huang Shui, Tiantang to Liancheng of the Datong He), (III) the LP sections (the drainage basins downstream Lijiacun of the Tao He, Xining of the Huang Shui, and Liancheng of the Datong He). The detailed latitude, longitude and elevation of the stations are in **Supplementary Table S1**.

also distributed with a small amount of granite derived from magmatic activity (**Figure 1B**, Wang and Chen, 1897; Pang et al., 2018). Loess containing evaporite and significant amounts of carbonate are also locally distributed in the Datong He QTP section (Chen et al., 2005).

The average elevation of the transition zones between the QTP and the LP drops from 4,000 to approximately 2,000 m. As the elevation decreases in the transition zones, the temperature rises, precipitation increases, and the climate changes to temperate semi-humid. The main industry gradually converts from pastoralism to agriculture. The transition zones of the three rivers are sporadically covered by loess (Pang et al., 2018). In addition to silicate and carbonate minerals (10–15%), the loess also contains a large amount of evaporite salts (5–10%), such as chlorides and sulfates (Zhang et al., 1995). Other rock types in the transition zones are similar to the QTP sections. It should be noted that the basin above Minxian of the Tao He mainly contains Triassic strata, while below Minxian strata such as Permian of an earlier age (Gansu Province 1:500,000 geological map, www.ngac.org.cn) dominates.

The average elevation of the LP sections is approximately 1,700 m. This area has little rain and a temperate continental climate, such that the ratio of evaporation to precipitation has reached 4.58 (1991–2000, Yang et al., 2004). The main industry is agriculture (Wang et al., 2012; Shichao et al., 2013).

2.2 Sampling and Analysis

The sampling stations are shown in **Figure 1**. Surveys were conducted in July 2013, October 2013, January 2014, and April 2014 at the outlets of the Tao He, Huang Shui, and Datong He. A whole-basin survey was conducted in August 2015 for each of the three rivers. Samples were also taken at the Lanzhou station on the Yellow River mainstream in all surveys. Water samples were collected in the middle of the river, approximately 50 cm below the surface, using floating bridges or boats. Cities and pollution sources were avoided when collecting the water samples.

The water samples for pH measurement were stored in polyethylene pre-cleaned bottles. The water samples for major ions were filtered through 0.45 μm cellulose acetate membrane filters and stored in pre-cleaned polyethylene bottles. The filtrate was divided into two parts: one part was acidified to pH < 2 with ultrapure 1:1 nitric acid for cation analysis (Na^+, K^+, Ca^{2+}, Mg^{2+}), and the non-acidified part was used for anion (SO_4^{2-}, Cl^-, NO_3^-) and dissolved silica (SiO_2) determination. Samples for dissolved inorganic carbon (DIC) measurements were first filtered through a 0.45 μm cellulose acetate membrane into a 20 ml glass vial and poisoned with saturated $HgCl_2$ (−0.02% of the filtrate volume; Dickson and Goyet, 1994). Samples were stored at 4°C before analysis and equilibrated to ambient temperature when analyzed.

The pH was determined with an Orion 3-Star Plus pH benchtop meter (Thermo Fisher Scientific Inc., Beverly, MA, USA) at a temperature of 25°C within 12 h of sampling. Before measurement, the pH meter was calibrated by the NIST standard. The measurement precision of pH was ±0.01. Cation analysis was done *via* atomic absorption spectrophotometry (AA240FS, Agilent Corporation, USA), calibrated by the standard solution from Sigma-Aldrich, while the anion analysis was *via* ion chromatography (ICS3000, Dionex Corporation, USA), calibrated by an anion standard (IC-FAS-1A, Inorganic Venture Inc., USA). The measurement errors of all ion concentrations were less than 1%. SiO_2 was measured with spectrophotometric measurements of the Mo blue complex, calibrated by Bellancom SiO_2 standard solution, and the measurement precision is better than 5%. The DIC samples were measured by a total organic carbon analyzer (TOC-VCPN, Shimadzu Corporation, Japan), corrected by the Standard Seawater (Batch 163) from Dickson Lab. The variance coefficient of the instrument was less than 1%. In this study, we used DIC values equal to the HCO_3^- concentrations. As in previous studies on chemical weathering, DIC is used values to represent HCO_3^- concentrations (Oh and Raymond, 2006; Wang et al., 2016). Samples for the total suspended solid (TSS) were assessed by weighing the material collected on the filter membranes by an electronic balance (AL 104, Mettler Toledo, Switzerland) at a precision of 0.0001 g. Total dissolved solids (TDS) were obtained by summing the concentration of measured ions and SiO_2.

2.3 Forward Model

Major dissolved ions in rivers are derived from atmospheric input, anthropogenic activities, and chemical weathering. When the Forward model is used to identify the contributions of different sources, the total amount of an element X in the rivers can be expressed as follows (Galy and France-lanord, 1999):

$$[X]_{riv} = [X]_{atm} + [X]_{ant} + [X]_{carb} + [X]_{sil} + [X]_{eva} + [X]_{sul} \quad (1)$$

where the subscripts denote riv, atm, ant, carb, sil, eva, and sul indicate river, atmospheric input, anthropogenic activity input, carbonate weathering, silicate weathering, evaporite dissolution, and sulfide oxidation, respectively. The ion concentration units in the calculation are molar concentrations.

2.3.1 Atmospheric Input

Atmospheric input of SO_4^{2-} was deducted using the proportion of 1.7% of total SO_4^{2-}, as reported by Zhang et al.'s (2020a) $\delta^{34}O_{SO_4}$, $\delta^{18}O_{SO_4}$ analysis of the source of sulfate in the Yellow River. For other ions, we used the method of Moquet et al. (2011) for deducting atmospheric inputs, which considers the ionic concentration of rainwater, precipitation, and runoff:

$$X_{atm} = (X/Cl^-)_{rain} \times Cl^-_{ave} \times P/R \quad (2)$$

where X_{atm} is the corrected concentration of the rainwater; $(X/Cl)_{rain}$ is the molar ratio in rainwater; Cl^-_{ave} is the average value of the Cl^- concentration of the rainwater in the basin; P is the precipitation in the basin (mm); and R is the runoff in the basin (mm).

The ionic concentration of rainwater was obtained from the China Global Atmosphere Watch Baseline Observatory at Waliguan, which is located on the northeast part of the QTP (Tang et al., 2000, **Supplementary Table S2**). According to the Yellow River Water Resources Bulletin[1], the average precipitation

[1]Yellow river conservancy commission of ministry of water resources. Yellow River Water Resources Bulletin. http://www.yrcc.gov.cn/zwzc/gzgb/gb/szygb/

and runoff in the Yellow River QTP sub-basin in 2013 and 2014 were 497 and 143 mm, respectively. Thus, the P/R ratio is 3.5. In the following, $^*X_{riv}$ represents the concentration of a certain ion after deducting the atmospheric input.

2.3.2 Silicate Weathering

2.3.2.1 K^+_{sil}

In addition to silicate weathering, $^*K^+_{riv}$ is also affected by the application of potassium fertilizers (Chetelat et al., 2008; Wang et al., 2016). For K^+ in the Yellow River from agricultural input, based on the average application ratio of 4.6:1 for nitrogen (by NO_3^-) and potassium (by K^+) fertilizers in the Yellow River basin, and the utilization ratios of 0.35 and 0.48 for nitrogen and potassium fertilizers, Wang et al. (2016) calculated a NO_3^-/K^+ (mol/mol) formed by excess nitrogen and potassium fertilizers to be about 5, and used this ratio to correct for the K^+ from agricultural input. We applied the same NO_3^-/K^+ ratio to correct the K^+ from agricultural input. The NO_3^-/K^+ ratios used in the Yangtze River basin were 3–4 (Chetelat et al., 2008). The K^+ in the three rivers derived from silicate weathering can be expressed as follows:

$$K^+_{sil} = {}^*K^+_{riv} - K^+_{agr} = {}^*K^+_{riv} - 1/5NO^-_3 \quad (3)$$

2.3.2.2 Na^+_{sil}

When K^+_{sil} value is available, Na^+_{sil} can be calculated from the $(K^+/Na^+)_{sil}$ ratio (Gaillardet et al., 1999). Wang et al. (2016) studied the chemical weathering in the Yellow River mainstream, considered the predominant distribution of shale above the Lajia station in the Yellow River source area (**Figure 1**) and the river water has a very low SO_4^{2-} concentration, suggested that the contribution of Na_2SO_4 to evaporite dissolution can be ignored. Therefore, the author obtained Na^+_{sil} at the Lajia station from the difference between the $^*Na^+_{riv}$ and $^*Cl^-_{riv}$, giving a $(K^+/Na^+)_{sil}$ ratio of 0.37 ± 0.03 for the other parts of the Yellow River (downstream of the Lajia station) to calculate the Na^+_{sil} in the river water. We used the same ratio to calculate the Na^+_{sil} for each station, which can be written as follows:

$$Na^+{}_{sil} = K^+{}_{sil}/0.37 \quad (4)$$

2.3.2.3 Ca^{2+}_{sil}, Mg^{2+}_{sil}

The Ca^{2+} and Mg^{2+} of river water derived from silicate weathering can be obtained using the $(Ca^{2+}/Na^+)_{sil}$ and $(Mg^{2+}/K^+)_{sil}$ molar ratios of the silicate in the watershed (Galy and France-Lanord, 1999):

$$Ca^{2+}{}_{sil} = Na^+{}_{sil} \times \left(Ca^{2+}/Na^+\right)_{sil} \quad (5)$$

$$Mg^{2+}{}_{sil} = K^+{}_{sil} \times \left(Mg^{2+}/K^+\right)_{sil} \quad (6)$$

The riverbed sand can represent the unweathered bedrock from the watershed and reflect the silicates' composition (Blum et al., 1998; Dellinger et al., 2014). Wu et al. (2008a) measured $(Ca^{2+}/Na^+)_{sil}$ and $(Mg^{2+}/K^+)_{sil}$ ratios of 0.26 and 0.67, respectively, in the riverbed sand above Lanzhou of the Yellow River, and obtained Ca^{2+}_{sil} and Mg^{2+}_{sil} by using Na^+_{sil} and K^+_{sil} from silicate weathering and these ratios. Wang et al. (2016) also used these ratios to calculate Ca^{2+}_{sil}, Mg^{2+}_{sil} at the Lanzhou station of the Yellow River. Therefore, we used the same ratios to calculate Ca^{2+}_{sil} and Mg^{2+}_{sil}.

2.3.3 Evaporite Dissolution

2.3.3.1 Na^+_{eva}

After subtracting Na^+_{sil} from $^*Na^+_{riv}$, almost all of the residual Na^+ in the river water comes from the dissolution of evaporites (NaCl and Na_2SO_4). Thus, Na^+_{eva} can be expressed as follows:

$$Na^+_{eva} = Na^+_{Na_2SO_4} + Na^+_{NaCl} = {}^*Na^+_{riv} - Na^+_{sil} \quad (7)$$

2.3.3.2 Ca^{2+}_{eva}, Mg^{2+}_{eva}

The Ca^{2+} and Mg^{2+} derived from evaporite dissolution are mainly from their corresponding sulfates ($CaSO_4$ and $MgSO_4$). In addition to the atmospheric inputs and sulfate dissolution, the SO_4^{2-} in the river could also be derived from pyrite oxidation (Torres et al., 2014). Previous studies on the Yellow River source area (Li et al., 2018) and the whole Yellow River basin (Fan et al., 2014; Wang et al., 2016) did not consider the contribution of pyrite oxidation to SO_4^{2-}. However, recently Zhang et al. (2020a) used $\delta^{34}O_{SO_4}$, $\delta^{18}O_{SO_4}$ to study the sulfate source in the Yellow River and measured $\delta^{34}O_{SO_4}$ of +4.7‰ and +7.3‰ and $\delta^{18}O_{SO_4}$ of +5.4‰ and +14.9‰ at the outlets of the Tao He and Huang Shui (including the Datong He), respectively, and obtained the proportion of sulfate originating from gypsum and pyrite oxidation as 76.6, 21.7 and 87.3, 11.0% respectively. We used these proportions to correct for SO_4^{2-} derived from pyrite oxidation in the respective rivers. After correcting for the contribution of pyrite oxidation and sodium sulphate dissolution to SO_4^{2-}, the Ca^{2+} and Mg^{2+} contributed by evaporite dissolution can be expressed as:

$$\begin{aligned}\left(Ca^{2+} + Mg^{2+}\right)_{eva} &= {}^*SO^{2-}_{4riv} - SO^{2-}_{4sul} - SO^{2-}_{4\ Na_2SO_4} \\ &= {}^*SO^{2-}_{4riv} - SO^{2-}_{4riv} \times f_{sul} - \left({}^*Na^+{}_{riv} - {}^*Cl^-{}_{riv} - Na^+{}_{sil}\right)/2\end{aligned} \quad (8)$$

where f_{sul} is the percentage contribution of pyrite oxidation to SO_4^{2-} in each river. $^*Cl^-_{riv}$ represents Na^+_{NaCl}. After correcting for atmospheric input the remaining Cl^- in the river water is derived from the halite (NaCl) dissolution.

2.3.4 Carbonate Weathering

The dissolved cations produced by carbonate weathering mainly include Ca^{2+}_{carb} and Mg^{2+}_{carb} from calcite and dolomite weathering. Ca^{2+}_{carb} and Mg^{2+}_{carb} can be obtained by subtracting the Ca^{2+} and Mg^{2+} from silicate weathering and evaporite dissolution from the $^*Ca^{2+}_{riv}$ and $^*Mg^{2+}_{riv}$:

$$\begin{aligned}\left(Ca^{2+} + Mg^{2+}\right)_{carb} = {}^*\left(Ca^{2+} + Mg^{2+}\right)_{riv} &- \left(Ca^{2+} + Mg^{2+}\right)_{sil} \\ &- \left(Ca^{2+} + Mg^{2+}\right)_{eva}\end{aligned} \quad (9)$$

2.4 Estimation of CO_2 Consumption, Chemical Weathering Rate of Silicate and Carbonate, and the Physical Erosion Rate

Bicarbonate ions generated from silicate weathering using carbonic acid are all derived from atmospheric CO_2, but half

of the bicarbonate ions generated from carbonate weathering using carbonic acid are from atmospheric CO_2. For basins where pyrite occurs, carbonate weathering by sulfuric acid also releases CO_2, and so the dissolved cations derived from chemical weathering by sulfuric acid need to be deducted when calculating the CO_2 consumption (Li et al., 2014; Torres et al., 2014; Zhang et al., 2020b). According to the method of Li et al. (2014), sulfuric acid consumed by silicate and carbonate weathering were calculated as follows:

$$SO_{4sul}^{2-} = SO_{4ssw}^{2-} + SO_{4csw}^{2-} \quad (10)$$

where the subscripts sul indicate sulfuric acid from oxidation of pyrite, ssw and csw indicate sulfuric acid consumed by silicate weathering, sulfuric acid consumed by carbonate weathering, respectively.

Assuming that silicate and carbonate weathering by sulphuric acid occur in the same ratio as those by carbonic acid (Galy and France-Lanord., 1999), the ratio can be written as follows:

$$R \approx SO_{4csw}^{2-}/SO_{4ssw}^{2-} = \left(Ca^{2+} + Mg^{2+}\right)_{carb} / \left(1/2Na^{+}_{sil} + 1/2K^{+}_{sil} + Ca^{2+}_{sil} + Mg^{2+}_{sil}\right) \quad (11)$$

where R is the ratio of sulphuric acid consumed by carbonate weathering to sulphuric acid consumed by silicate weathering; subscripts carb and sil represent carbonate weathering and silicate weathering, respectively.

With combining **Equations 10**, **11** to obtain SO_{4ssw}^{2-} and SO_{4csw}^{2-}, the dissolved cations generated from silicate and carbonate weathering by sulfuric acid can be expressed as (Spence and Telmer, 2005):

$$SO_{4ssw}^{2-} = 1/2Na^{+}_{ssw} + 1/2K^{+}_{ssw} + Ca^{2+}_{ssw} + Mg^{2+}_{ssw} \quad (12)$$

$$SO_{4csw}^{2-} = \left(Ca^{2+} + Mg^{2+}\right)_{csw}/2 \quad (13)$$

The CO_2 consumption by chemical weathering can be calculated based on the charge balance after deducting the contribution of dissolved cations from chemical weathering by sulfuric acid (Li et al., 2014):

$$F_{CO_2 sil} = \left(Na^{+}_{sil} + K^{+}_{sil} + 2Ca^{2+}_{sil} + 2Mg^{2+}_{sil} - 2SO_4^{2-}{}_{ssw}\right) \times Q \quad (14)$$

$$\Phi_{CO_2 sil} = F_{CO_2 sil}/A \quad (15)$$

$$F_{CO_2 carb} = \left(Ca^{2+}{}_{carb} + Mg^{2+}{}_{carb} - SO_4^{2-}{}_{csw}\right) \times Q \quad (16)$$

$$\Phi_{CO_2 carb} = F_{CO_2 carb}/A \quad (17)$$

where F_{CO_2} and Φ_{CO_2} stand for chemical weathering CO_2 consumption flux and rate by carbonic acid, respectively; Q is the discharge; and A denotes the basin area.

In order to obtain CO_2 consumption by chemical weathering in each sub-basin with different lithologies, Wang et al. (2016) divided the Yellow River mainstream into the QTP sub-basin, LP sub-basin, and lower sub-basin, and calculated the CO_2 consumption by chemical weathering separately. Following the method of Wang et al. (2016), the Tao He, Huang Shui, and Datong He were divided into the QTP section (I), the transition zone between the QTP and the LP (II), and the LP section (III) based on careful consideration of elevation and lithological distribution (**Figure 1B**), and quantified the CO_2 consumption by chemical weathering in sections with different lithological distributions, respectively. In the piecewise calculation, the ions in a given section mainly come from the chemical weathering in that section and from upstream input, while the output of the ions is transported downstream (**Figure 2**).

Equations for piecewise calculation of the CO_2 consumption fluxes and rates by chemical weathering are as follows:

$$F_{CO_2 i} = F_{CO_2 out,i} - F_{CO_2 in,i} \quad (18)$$

$$\Phi_{CO_2 i} = F_{CO_2 i}/A_i \quad (19)$$

$$F_{CO_2} = \sum F_{CO_2 i} \quad (20)$$

$$\Phi_{CO_2} = F_{CO_2}/A \quad (21)$$

where i represents the section of the river, and out and in indicate the outlet and inlet of the section, respectively.

The total, carbonate and silicate chemical weathering rates (TWR, CWR, and SWR) can be estimated as follows:

$$SWR = \left(Na^{+}_{sil} + K^{+}_{sil} + Ca^{2+}_{sil} + Mg^{2+}_{sil} + SiO_2\right) \times Q/A \quad (22)$$

$$CWR = \left(Ca^{2+}_{carb} + Mg^{2+}_{carb} + 1/2HCO^{3-}_{carb}\right) \times Q/A \quad (23)$$

$$TWR = SWR + CWR \quad (24)$$

It should be noted that the ion concentration units in **Equations 22**, **23** are mass concentrations.

The physical erosion rate (PER) can be expressed as:

$$PER = TSS \times Q/A \quad (25)$$

where TSS is the total suspended solid, in mass concentration.

The total denudation rate (TDR) can be written as:

$$TDR = PER + TWR \quad (26)$$

2.5 Statistical Analyses

The average values are reported with ±standard deviation (S.D.). The correlations between two variables were analyzed using the SPSS 21 software (IBM SPSS Statistics, IBM Corporation, Armonk, New York, NY), and the statistical analyses all had a significance level of 0.05.

3 RESULTS

3.1 Field Measurements

The water in the Tao He, Huang Shui, and Datong He is weakly alkaline with pH values varying from 8.02 to 8.61 (**Table 1**, **2**). The average TDS in each basin in summer were 306 ± 18, 449 ± 137, 327 ± 17 mg L^{-1} in the Tao He, Huang Shui, and Datong He, respectively. The average TDS values in all four seasons at the outlet were 413 ± 76, 865 ± 220, 318 ± 29 mg L^{-1} for the Tao He, Huang Shui, and Datong He, respectively. The average TDS value at the Lanzhou station (413 ± 50 mg L^{-1}) on the mainstream of the Yellow River was similar to that of the Tao He, half that of the Huang Shui, and higher than that of the Datong He. Except for

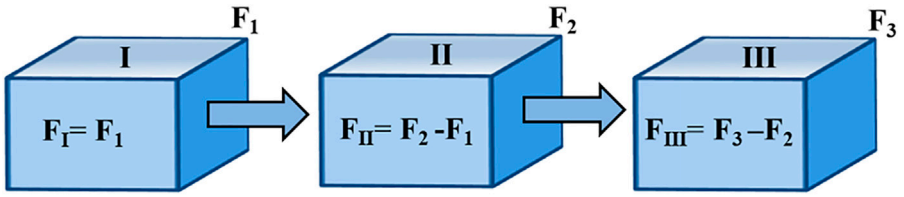

FIGURE 2 | CO_2 consumption flux by chemical weathering in different sections (Modified from Wang et al., 2016). I represents the QTP section, II represents the transition zone between the QTP and the LP, and III represents the LP section.

the summer measurement of 2013 at the outlet of the Datong He, all of the TDS values were higher than the average value for the world's rivers (283 mg L^{-1}, Han and Liu, 2004). The total dissolved cation charge ($TZ^+ = Na^+ + K^+ + 2Mg^{2+} + 2Ca^{2+}$) and total dissolved anion charge ($TZ^- = Cl^- + NO_3^- + 2SO_4^{2-} + HCO_3^-$) of each sample were basically balanced, and most samples had normalized inorganic charge balances (NICBs) within ±10%, which indicated that the influence from other unknown ions was small.

As seen in **Tables 1** and **2**, HCO_3^- was the dominant anion in the Tao He, Huang Shui, and Datong He, with concentrations of 3,418 ± 250, 3,433 ± 577, and 3,140 ± 287 μmol L^{-1} (the average value of the outlet in four seasons and all stations during the summer in each river, respectively. The same calculation was used to obtain the following values). The HCO_3^- concentrations of the Tao He and Huang Shui were higher than that at the Lanzhou station on the mainstream of the Yellow River (3,220 ± 170 μmol L^{-1}). Followed by the concentrations of $Cl^- + SO_4^{2-}$, which were 680 ± 573, 4,012 ± 2,685, 571 ± 193 μmol L^{-1} for the Tao He, Huang Shui, and Datong He, respectively. Only the $Cl^- + SO_4^{2-}$ concentration of the Huang Shui exceeded that at the Lanzhou station (1,526 ± 495 μmol L^{-1}). The major dissolved cations in the three rivers were Ca^{2+} and Na^+, with concentrations of 1,439 ± 288 and 620 ± 509 μmol L^{-1} in the Tao He, 2,167 ± 635 and 3,608 ± 2,741 μmol L^{-1} in the Huang Shui, and 1,413 ± 168 and 435 ± 86 μmol L^{-1} in the Datong He. Similarly, only the Ca^{2+} and Na^+ concentrations of the Huang Shui were higher than those of the Lanzhou station (1,529 ± 122 and 1,327 ± 417 μmol L^{-1}, respectively). In addition, the NO_3^- concentrations of the three rivers, which were strongly influenced by agricultural activities, all exhibited an increasing trend from upstream to downstream (12–475 μmol L^{-1}).

3.2 Hydrochemistry Type

Hydrochemical data for the Tao He, Huang Shui and Datong He (blue symbols) together with the mainstream of the Yellow River (black symbols) are plotted in **Figure 3** to illustrate the changing ion composition downstream. From upstream to downstream of the Yellow River mainstream, the proportions of Ca^{2+} and HCO_3^- gradually decrease, and the proportions of $Na^+ + K^+$ and $Cl^- + SO_4^{2-}$ gradually increase. The highest proportions of Ca^{2+} and HCO_3^- (unfilled black symbols) occurred in the shale-dominated source area (upstream of the Tangnaihai station, **Figure 1**). However, due to evaporite dissolution input in the section from Tangnaihai to Lanzhou, the proportions of $Na^+ + K^+$ and $Cl^- + SO_4^{2-}$ increase significantly (black crosses). The hydrochemistry type upstream of the Lanzhou station is Ca^{2+}-HCO_3^-. After entering the hinterland of the LP (downstream of the Lanzhou station), evaporite dissolution becomes the primary source of ions (unfilled black triangles), the proportions of $Na^+ + K^+$ and $Cl^- + SO_4^{2-}$ become higher downstream, and the hydrochemistry type changes from Ca^{2+}-HCO_3^- to Na^+-$Cl^- + SO_4^{2-}$.

The hydrochemistry type of the Tao He and Datong He are similar to that of the Yellow River source area (**Figure 3**), which is Ca^{2+}-HCO_3^-. For the Huang Shui, only the hydrochemistry type upstream of the Haiyan station is Ca^{2+}-HCO_3^-. From the Huangyuan station in the midstream to the outlet, the hydrochemistry changes similar to that below Tangnaihai station in the mainstream of the Yellow River, showing that the proportions of $Na^+ + K^+$ and $Cl^- + SO_4^{2-}$ gradually increase, and the hydrochemistry type gradually changes from Ca^{2+}-HCO_3^- upstream to Na^+-$Cl^- + SO_4^{2-}$ downstream. In addition, the SiO_2 contents of the three rivers are consistently low.

3.3 Contributions of Different Sources to Dissolved Cations

Figure 4 shows the contributions of the different sources to dissolved cations in the three rivers. These values were calculated using the Forward model after deducting the input from agricultural fertilization. The contributions from carbonate weathering to dissolved cations in the Tao He, Huang Shui, and Datong He decrease from 90, 67, and 70% at their sources to 75, 37, and 66% at their outlets, respectively. Meanwhile, contributions from evaporite dissolution to dissolved cations increase from 4, 24, and 24% at their sources to 18, 59, and 28% at their outlets, respectively. It can be seen that the dissolved cations in the Tao He and Datong He are mainly from carbonate weathering, while those of the Huang Shui is dominated by evaporite dissolution. The contributions of silicate weathering and atmospheric inputs to the dissolved cations in the three rivers are relatively small, ranging from 1 to 4% and 3 to 6%, respectively.

It should to be noted that there are some uncertainties in calculating ions from different weathering source by using the Forward model. The most prominent example is that when calculating the Ca^{2+} and Mg^{2+} from silicate weathering using the $(Ca^{2+}/Na^+)_{sil}$ and $(Mg^{2+}/K^+)_{sil}$ ratios with ±50% uncertainty obtained from riverbed sand, commonly used in studies (Galy

TABLE 1 | Dissolved chemical composition for the Tao He, Huang Shui, and Datong He and the Lanzhou station on the Yellow River mainstream in summer.

Basin	Station	Sampling date	Elevation	River length	pH	Na^+	K^+	Mg^{2+}	Ca^{2+}	Cl^-	SO_4^{2-}	NO_3^-	HCO_3^-	SiO_2	TDS[a]	TSS	NICB[b]
		dd/mm/yy	m	km		μmol L^{-1}									mg L^{-1}		%
Tao He	Luqu	28/07/2015	3,164	61	8.45	154	22	668	1,267	82	69	16	3,707	124	315	34	2.5%
	Xiabagou	29/07/2015	2,536	254	8.48	214	32	568	1,254	119	76	26	3,484	115	303	21	2.8%
	Minxian	30/07/2015	2,307	335	8.41	218	31	517	1,185	144	102	43	3,290	127	292	49	–0.7%
	Lijiacun	30/07/2015	1,918	493	8.35	246	34	502	1,192	138	130	54	3,144	130	287	214	2.0%
	Hongqi[c]	30/07/2015	1,787	673	8.27	641	42	585	1,270	372	299	85	3,188	136	331	720	3.4%
Huang Shui	Haiyan	04/08/2015	2,994	40	8.24	952	52	502	1,531	792	265	26	3,162	155	355	86	11.0%
	Huangyuan	04/08/2015	2,635	79	8.45	1,259	61	478	1,537	1,156	365	73	2,960	130	373	1,589	8.0%
	Xining	02/08/2015	2,229	132	8.20	1,617	72	573	1,645	1,368	792	149	2,578	138	419	9,950	7.3%
	Minhe[c]	01/08/2015	1,766	374	8.02	3,371	110	883	2,075	2,774	1,575	340	3,002	178	651	1,077	1.4%
Datong He	Tiantang	02/08/2015	2,348	461	8.61	333	30	618	1,159	175	446	56	3,006	118	313	25	–5.4%
	Liancheng	01/08/2015	1,871	521	8.52	450	34	671	1,241	277	482	64	2,985	131	327	138	0.4%
	Xiangtang[c]	01/08/2015	1,759	561	8.50	521	36	696	1,343	286	592	69	3,025	133	348	209	1.5%
Yellow River mainstream	Lanzhou	31/07/2015	1,515	2,119	8.28	1,043	54	659	1,341	705	608	85	3,053	153	380	331	0.7%

[a] $TDS = Na^+ + K^+ + Mg^{2+} + Ca^{2+} + Cl^- + NO_3^- + SO_4^{2-} + HCO_3^- + SiO_2$

[b] $NICB = (TZ^+ - TZ^-)/TZ^+$, $TZ^+ = Na^+ + K^+ + 2Mg^{2+} + 2Ca^{2+}$, $TZ^- = Cl^- + NO_3^- + 2SO_4^{2-} + HCO_3^-$

[c] River outlet.

and France-Lanord, 1999; Singh et al., 2005; Wu et al., 2008a; Jiang et al., 2018), it would bring an uncertainty of about ±22 and ±1% to the estimated cation from the silicate weathering and carbonate weathering, respectively. There are also uncertainties relating to the NO_3^-/K^+ ratio used to calculate the K^+ from agricultural fertilization in river water, the $(K^+/Na^+)_{sil}$ ratio used to calculate Na^+ from silicate weathering, and f_{sul} (percentage contribution of pyrite oxidation to SO_4^{2-}) used to deduct the contribution of SO_4^{2-} from pyrite oxidation, which can all cause some errors in calculating the ions from different weathering source.

3.4 CO_2 Consumption by Chemical Weathering

CO_2 consumption rates by chemical weathering of the Tao He, Huang Shui, and Datong He in summer are shown in **Table 3** (piecewise calculation, discussed in **Section 2.4**). The CO_2 consumption rates of carbonate weathering in the Tao He and Huang Shui are the highest in the transition zones between the QTP and the LP, followed by the QTP sections and the lowest in the LP sections. In contrast, the CO_2 consumption rates of carbonate weathering along the Datong He are as follows: the QTP section > the LP section > the transition zone.

The CO_2 consumption rates of silicate weathering in the Tao He in summer showed less variation and was lower than those of the other two rivers (**Table 3**). The CO_2 consumption rate of silicate weathering in the QTP section of the Huang Shui was lower than that in the transition zone between the QTP and the LP, but significantly higher than that in the LP section. For the Datong He, the CO_2 consumption rates of silicate weathering showed a gradual increase from the QTP section to the LP section.

The total CO_2 consumption flux of carbonate and silicate weathering in summer of the three rivers is the highest in the Tao He (19.97×10^8 mol a^{-1}), followed by the Datong He (17.70×10^8 mol a^{-1}), and the lowest in the Huang Shui (16.31×10^8 mol a^{-1}) (**Table 3**).

Based on seasonal variations in CO_2 consumption rates by chemical weathering at the outlets of the three rivers (**Table 4**), the CO_2 consumption rates of carbonate weathering for the Tao He and Datong He in summer are much higher than those in other seasons. However, except for the relatively low CO_2 consumption rate of carbonate weathering for the Huang Shui in winter, the differences between other seasons were small and were about two times higher than that in winter. The CO_2 consumption rate of silicate weathering was highest in summer for the Datong He, in autumn and summer for the Tao He, and in autumn for the Huang Shui. The annual CO_2 consumption rates of carbonate weathering at the outlets of the three rivers were all higher than that at the Lanzhou station on the mainstream of the Yellow River. However, only the annual CO_2 consumption rate of silicate weathering for the Huang Shui was higher than that at the Lanzhou station.

Although the area of these three rivers only accounts for 25% of the Yellow River QTP sub-basin, their contribution to the total CO_2 consumption flux by chemical weathering approximates

TABLE 2 | Seasonal dissolved chemical composition at the outlets of the Tao He, Huang Shui, and Datong He and the Lanzhou station on the Yellow River mainstream.

Basin	Station	Season	Sampling date	pH	Na^+	K^+	Mg^{2+}	Ca^{2+}	Cl^-	SO_4^{2-}	NO_3^-	HCO_3^-	SiO_2	TDS[a]	TSS	NICB[b]
			dd/mm/yy						μmol L^{-1}					mg L^{-1}		%
Tao He	Hongqi[c]	Summer	02/07/2013	8.55	437	36	371	1,394	175	287	36	3,159	117	312	438	1.4%
		Autumn	01/10/2013	8.48	1,038	66	606	1,829	476	787	89	3,375	152	427	108	7.7%
		Winter	08/01/2014	8.48	1,627	35	787	1,949	856	908	12	3,836	117	495	62	8.6%
		Spring	06/04/2014	8.32	1,002	55	696	1,613	437	682	95	3,576	140	420	40	3.6%
Huang Shui	Minhe[c]	Summer	02/07/2013	8.16	3,012	132	695	2,361	2,333	1,768	264	3,845	167	699	1,597	−7.8%
		Autumn	01/10/2013	8.10	4,334	160	849	2,874	3,127	2,255	159	4,001	154	832	1,227	1.2%
		Winter	08/01/2014	8.23	9,382	170	1,040	3,259	6,130	3,369	95	4,153	110	1,185	154	5.7%
		Spring	06/04/2014	8.13	4,938	120	986	2,058	2,155	1,877	475	3,763	102	746	286	9.0%
Datong He	Xiangtang[c]	Summer	02/07/2013	8.37	316	50	372	1,476	190	149	47	2,840	113	281	297	16.9%
		Autumn	01/10/2013	8.47	414	53	391	1,606	330	167	51	3,032	147	310	179	16.0%
		Winter	08/01/2014	8.45	472	37	442	1,503	197	209	15	3,596	147	339	74	4.0%
		Spring	06/04/2014	8.32	535	44	420	1,560	325	170	95	3,498	139	342	137	6.2%
Yellow River mainstream	Lanzhou	Summer	02/07/2013	8.28	904	67	424	1,476	534	406	62	3,041	125	347	550	6.7%
		Autumn	30/09/2013	8.35	1,238	69	512	1,634	819	585	59	3,235	128	403	340	5.7%
		Winter	07/01/2014	8.45	1,963	51	544	1,624	1,163	737	15	3,397	96	451	98	4.8%
		Spring	05/04/2014	8.22	1,486	60	496	1,568	1,317	757	135	3,376	114	452	161	−11.8%

[a] $TDS = Na^+ + K^+ + Mg^{2+} + Ca^{2+} + Cl^- + NO_3^- + SO_4^{2-} + HCO_3^- + SiO_2$

[b] $NICB = (TZ^+ - TZ^-)/TZ^+$, $TZ^+ = Na^+ + K^+ + 2Mg^{2+} + 2Ca^{2+}$, $TZ^- = Cl^- + NO_3^- + 2SO_4^{2-} + HCO_3^-$

[c] *River outlet.*

36% (36% for carbonate weathering, 29% for silicate weathering), which is 177.75 × 10^8 mol a^{-1} (Tao He: 92.81 × 10^8 mol a^{-1}, Huang Shui: 39.60 × 10^8 mol a^{-1}, Datong He: 45.16 × 10^8 mol a^{-1}). Among the three rivers, the total annual CO_2 consumption flux by chemical weathering in the Tao He accounts for 52% of the contribution of the three rivers to the Lanzhou station.

4 DISCUSSION

4.1 Main Factors Controlling the Chemical Weathering in the Tao He, Huang Shui, and Datong He

The QTP sections and the transition zones between the QTP and the LP of the Tao He, Huang Shui, and Datong He have high chemical weathering rates, which are the main contributors to the CO_2 consumption fluxes in these drainage basins.

The QTP sections are dominated by shale (**Figure 1B**), but the CO_2 consumption rates of carbonate weathering are more than one magnitude higher than those of silicate weathering (**Table 3**). This may be related to a small amount of carbonate contained in shale (Wu et al., 2008a), as carbonate has faster dissolution kinetics than silicate (Kump et al., 2000). Even the amount of carbonate in the bedrock is minimal and the drainage basin is dominated by carbonate weathering (Blum et al., 1998). The CO_2 consumption rate of carbonate weathering in the QTP section of the Datong He is significantly higher than that in the Tao He and Huang Shui. This is related to locally exposed carbonate and loess in the QTP section of the Datong He, and this section is also the main discharge-producing region of this basin. In terms of silicate weathering in the QTP sections (**Table 3**), the CO_2 consumption rate of silicate weathering in the Tao He is significantly higher than that in the Datong He. Because the QTP section of the Tao He is mainly composed of shale and sandstone, while in addition to shale, the QTP section of the Datong He has gneiss and schist (**Figure 1B**), whose weathering rates are only 0.4 times that of shale (Meybeck, 1987). Although the QTP section of the Huang Shui is also dominated by gneiss and schist, the calculated CO_2 consumption rate of silicate weathering is much higher than that of the Tao He and Datong He (**Table 3**). This most likely relates to hot spring input, which is often an essential source of silicate ions in the watershed (Evens et al., 2004). Hot springs are widespread on the margins of the QTP (Zhou et al., 2012) and are distributed in the Huang Shui basin (Tan et al., 2012). However, due to the lack of sufficient data, we did not correct the ions from hot spring input when estimating the CO_2 consumption by chemical weathering.

Figure 5 shows that the highest CO_2 consumption rate of carbonate weathering for both the Tao He and Huang Shui appear in the transition zones between the QTP and the LP where the relief ratios (relief/basin length) and runoff (water discharge/surface area) are high. The transition zones experience a sharp drop in elevation and a highly tattered landform, resulting in a significant increase in the physical erosion rate (PER, **Figure 6A**), and thus providing ample weathering materials. Meanwhile, the climate of the transition zones changes from subalpine semi-arid to temperate semi-humid, and runoff increases. All of these factors facilitate chemical weathering. As a result, the CO_2 consumption rates of carbonate weathering in the transition zones are significantly higher than those in the QTP sections, and much higher than those in the LP sections (**Table 3**), where there is gentle terrain and an arid climate. The ratio of the total chemical weathering rate (TWR) to the total denudation rate (TDR) (**Figure 6B**), shows that TWR dominates TDR in the QTP section, indicating the supply of weathering materials is insufficient and chemical weathering is in a "transport-limited" situation (West et al., 2005; Gabet et al., 2010). However, the TWR/TDR ratio of the Tao He transition zone is close to 50%,

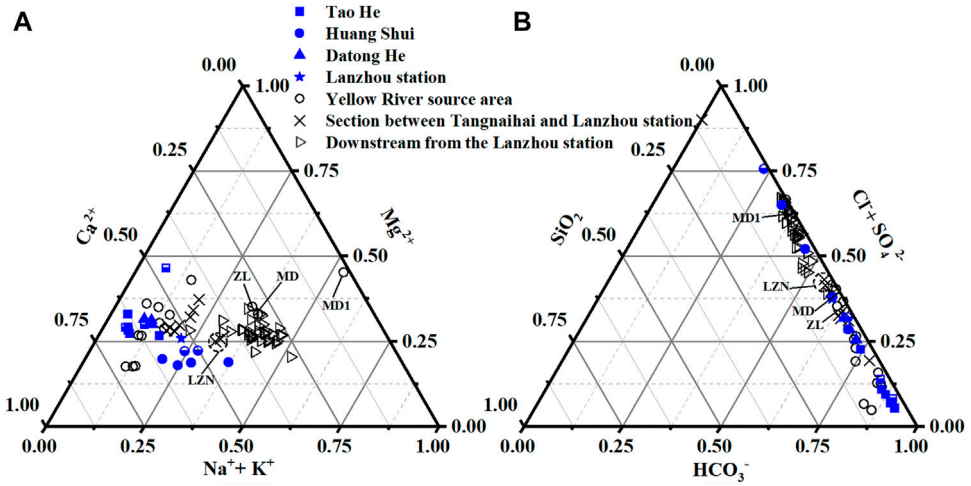

FIGURE 3 | Ternary plots of the **(A)** major cations and **(B)** anions-silica for the Tao He, Huang Shui, and Datong He (blue symbols) and the Lanzhou station on the Yellow River mainstream (blue stars) in summer (in μEq units). The solid blue symbols represent data collected in this study, and the half-filled blue symbols represent data from Wu et al. (2005). The black symbols are data from the Yellow River mainstream obtained from Wu et al. (2005), Fan et al. (2014), and Wang et al. (2016). The symbols marked in the figure are MD 1 (Maduo1), ZL (Lake Zaling), and MD (Maduo) are all located in the source area of the Yellow River in the Maduo territory. Because of thin-bedded halite deposits (Zheng, 1997), the proportion of $Na^+ + K^+$ is extremely high. In addition, data reported by Wu et al. (2005) were collected at the Lanzhou station during the non-flood season (LZN) in May and June, which caused exceedingly higher proportions of $Na^+ + K^+$ and $Cl^- + SO_4^{2-}$. However, other data in **Figure 3** were collected during the flood season in July and/or August.

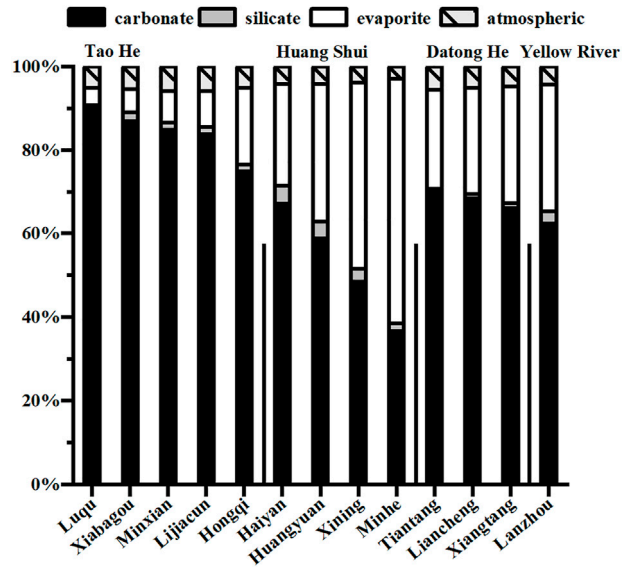

FIGURE 4 | Diagram showing the proportional contributions of the different sources to dissolved cations in summer. Data for contributions of different sources to dissolved cations are in **Supplementary Table S3**.

and so the weathering materials, as well as the climatic factors (temperature and runoff), have great influence on chemical weathering. The physical erosion rate (PER) of the Huang Shui transition zone is extremely high (**Figure 6A**) due to the widespread distribution of loess (**Figure 1B**), and the TWR/TDR ratio is extremely low (**Figure 6B**). With sufficient supply of weathering materials, the chemical weathering rate is limited by the kinetics of weathering reactions, defined as "kinetic-limited" (West et al., 2005; Gupta et al., 2011). Due to the great increase in runoff of the Huang Shui transition zone compared to the QTP section, it leads to a higher CO_2 consumption rate of carbonate weathering in the transition zone than that in the QTP section (**Table 3**). In the LP section of the Tao He and Huang Shui, the higher physical erosion rate (PER) (**Figure 6A**) leads to relatively low TWR/TDR (**Figure 6B**), and chemical weathering is in "kinetic-limited" situation mainly influenced by temperature, runoff and other climatic factors. The limited increase in runoff (**Table 3**) is the main reason for the low CO_2 consumption rate of carbonate weathering in the LP section.

However, for the Datong He, the CO_2 consumption rate of carbonate weathering in the transition zone with a relatively high relief ratio is lower than that in the LP section (**Figure 5A**). We notice that the increase of physical erosion rate (PER) in the Datong River LP section is not significant (**Figure 6A**), and the TWR/TDR ratios in its transition zone and LP section are around 50% (**Figure 6B**). Weathering materials, as well as temperature, runoff and other climatic environmental factors all have a high influence on chemical weathering. The lowest increase in runoff was observed in the LP section of the Datong He among the three rivers (**Table 3**), and the low physical erosion rate (PER) was associated with this. The CO_2 consumption rate of carbonate weathering in the LP section of the Datong He is more than double that in the Tao He and Huang Shui (**Table 3**). For the LP sections of the three rivers, slight differences in lithology and runoff would not lead to striking differences in CO_2 consumption rates of carbonate weathering within a limited area. The possible reason for this is that the Datong He transition zone has a river length of less than 60 km, with the relief ratio reaching 8‰

TABLE 3 | CO_2 consumption by chemical weathering of the Tao He, Huang Shui, Datong He, and the Lanzhou station on the Yellow River mainstream in summer (June to August).

Basin	Section	Area (10^4 km^2)	Natural discharge in summer (10^8 m^3)	$F_{CO_2 sil}$ (10^8 mol a^{-1})	$F_{CO_2 carb}$ (10^8 mol a^{-1})	$\Phi_{CO_2 sil}$ (10^3 mol km^{-2}a^{-1})	$\Phi_{CO_2 carb}$ (10^3 mol km^{-2}a^{-1})
Tao He	I	0.90	3.23	0.28	5.40	3.16	59.94
	II	1.07	9.54	0.32	9.00	3.02	84.17
	III	0.53	10.71	0.15	2.53	2.86	47.99
	Entire basin	2.50	10.71	0.76	16.93	3.04	67.78
Huang Shui	I	0.07	0.21	0.05	0.35	6.31	49.25
	II	0.83	5.12	0.86	6.84	10.39	82.30
	III	0.63	6.16	0.13	2.38	1.99	37.71
	Entire basin	1.53	6.16	1.03	9.57	6.74	62.39
Datong He	I	1.26	9.12	0.32	12.02	2.55	95.63
	II	0.13	9.17	0.12	0.98	8.59	73.37
	III	0.12	9.60	0.11	1.07	9.34	87.98
	Entire basin	1.51	9.60	0.55	14.07	3.63	93.05
Yellow River	Lanzhou	22.26	86.11	11.75	123.13	5.28	55.31

Natural discharge refers to river discharge without anthropogenic activity disturbances, equal to the sum of the measured discharge, water consumption, and reservoir storage variables (Wang et al., 2006). Measured discharge data were obtained from the National Water and Rain Information Network (http://xxfb.mwr.cn/). The data on water consumption and reservoir storage variables for the Tao He, Huang Shui, and Datong He were obtained from the Gansu Water Resources Bulletin[2], the Qinghai Water Resources Bulletin, and the Yellow River Water Resources Bulletin. According to the average annual discharge ratio at the Xiabagou and Hongqi stations for the Tao He from 1956 to 2006 (Zhu et al., 2012), and the discharge data at the Hongqi station during the sampling period, we apply the discharge ratio to obtain the absence discharge data of the Xiabagou station.

TABLE 4 | CO_2 consumption by chemical weathering at the outlets of the Tao He, Huang Shui, and Datong He, and Lanzhou station on the Yellow River mainstream in four seasons.

Basin	Station	Season	Area (10^4 km^2)	Natural discharge (10^8 m^{3}a^{-1})	$F_{CO_2 sil}$ (10^8 mol a^{-1})	$F_{CO_2 carb}$ (10^8 mol a^{-1})	$\Phi_{CO_2 sil}$ (10^3 mol km^{-2}a^{-1})	$\Phi_{CO_2 carb}$ (10^3 mol km^{-2}a^{-1})
Tao He	Hongqi	Summer	2.50	25.2	2.34	37.53	9.37	150.13
		Autumn	2.50	11.8	2.42	20.92	9.67	83.66
		Winter	2.50	4.9	0.55	10.27	2.21	41.09
		Spring	2.50	9.8	1.34	17.44	5.37	69.75
		Whole year	2.50	51.6	6.65	86.16	26.62	344.64
Huang Shui	Minhe	Summer	1.53	5.8	2.19	8.22	14.30	53.71
		Autumn	1.53	5.4	3.57	9.46	23.31	61.86
		Winter	1.53	2.0	1.55	4.42	10.16	28.87
		Spring	1.53	4.0	0.28	9.90	1.83	64.74
		Whole year	1.53	17.3	7.59	32.01	49.60	209.18
Datong He	Xiangtang	Summer	1.51	11.9	2.07	19.11	13.72	126.57
		Autumn	1.51	7.7	1.43	13.18	9.47	87.25
		Winter	1.51	2.4	0.32	4.17	2.12	27.60
		Spring	1.51	2.6	0.20	4.68	1.31	31.00
		Whole year	1.51	24.6	4.02	41.14	26.62	272.43
Yellow River	Lanzhou	Summer	22.26	110.4	27.31	165.34	12.27	74.28
		Autumn	22.26	77.2	20.04	122.59	9.00	55.07
		Winter	22.26	41.7	8.43	69.84	3.79	31.38
		Spring	22.26	64.2	7.05	81.83	3.17	36.76
		Whole year	22.26	293.6	62.83	439.60	28.22	197.48

Data from June 2014 was used due to a lack of discharge data for June 2013.

(**Table 1**, **Supplementary Table S4**). Such a high relief ratio reduces the water's residence time, and thus large quantities of fine-grained materials produced by the intense physical erosion in this section are delivered downstream without sufficient weathering. These materials may undergo extensive weathering after they are delivered to the gentle LP section. A similar situation occurs in the Ganges, where the downstream Gangetic plain has a higher chemical weathering rate than the upper and middle mountainous areas (West et al., 2002; Gabet and Mudd, 2009).

Variation of CO_2 consumption rates of silicate weathering in the transition zones of the Huang Shui and Datong He is consistent with carbonate weathering. Huang Shui has the highest CO_2 consumption rate by silicate weathering in the transition zone due to its high relief ratio and runoff (**Figures 5A,B**). As for the Datong He, it exhibits a lower CO_2

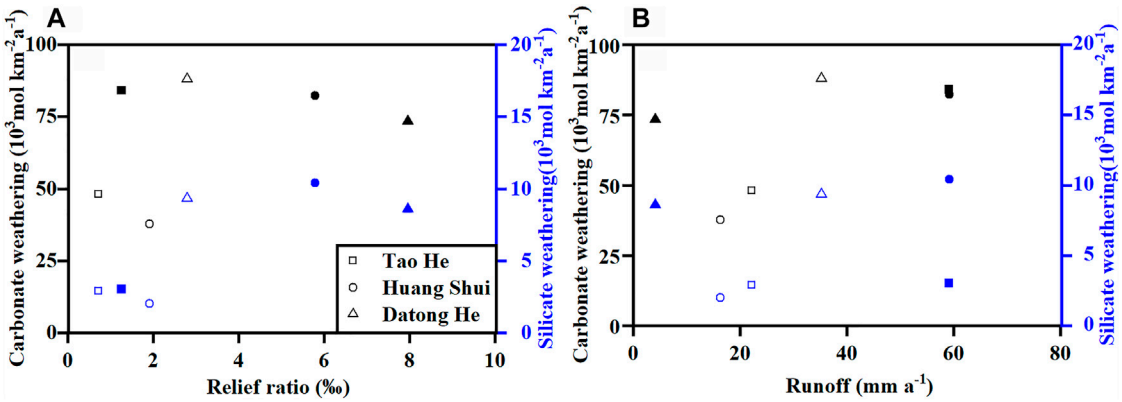

FIGURE 5 | Relationships between the CO_2 consumption rates of carbonate (black symbols) and silicate (blue symbols) weathering and **(A)** the relief ratio (relief/basin length) and **(B)** runoff (water discharge/surface area) in the transition zones and the LP sections of the Tao He, Huang Shui, and Datong He in summer. The solid symbols represent the transition zone. The unfilled symbols represent the LP section. In this paper, river length is substituted for basin length. Data for relief ratio and runoff are in **Supplementary Table S4**.

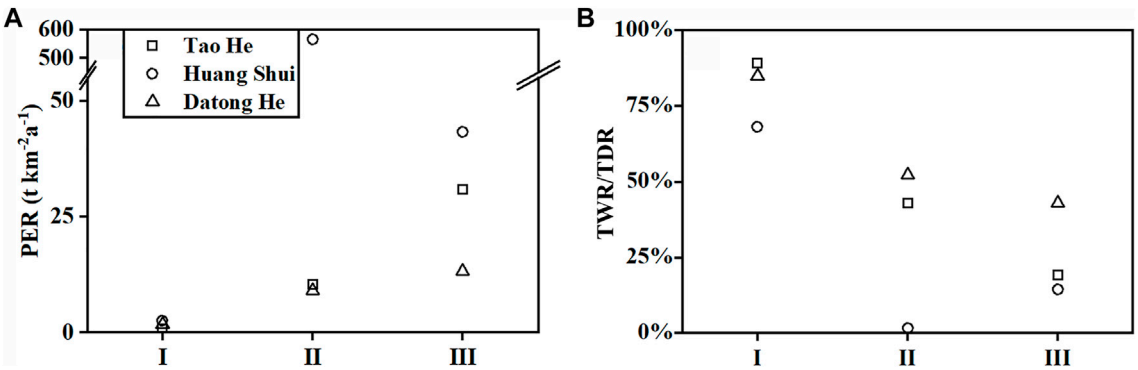

FIGURE 6 | Physical denudation rate (PER) **(A)** and the ratio of total chemical weathering rate (TWR) to total denudation rate (TDR) (TDR = TWR + PER) **(B)** of Tao He, Huang Shui, and Datong He. I represents the QTP section, II represents the transition zones, and III represents LP section, and data are shown in **Supplementary Table S6**.

consumption rate of silicate weathering in the transition zone than downstream LP section because the fine-grained weathering materials are transported downstream without sufficient weathering due to the high relief ratio. However, the CO_2 consumption rate of silicate weathering in the Tao He does not show a high value in the transition zone, like carbonate weathering, and remains almost unchanged as the relief ratio and runoff increase (**Figures 5A,B**). The geological information that can be accessed at present shows that although the Tao He transition zone is dominated by shale and sandstone, the basin above Minxian belongs to the Triassic strata, and the basin below Minxian belongs to the Permian strata of an earlier age (Gansu Province 1:500,000 geological map, www.ngac.org.cn). Judging from the age of land surfaces, the highly leached old surfaces can no longer produce high chemical yields (Blum, 1997). This is probably one of the reasons for the low CO_2 consumption rate of silicate weathering in the transition zone of the Tao He, which requires further study.

Consequently, it appears that the transition zones between the QTP and the LP contribute the most to the CO_2 consumption by chemical weathering in these basins. The total CO_2 consumption rates by chemical weathering in the Tao He and Huang Shui transition zones are 1.4 times and 1.7 times greater than in their QTP sections, and 1.5 times and 2.0 times greater than in their LP sections, respectively. However, the relief ratio in the Datong He transition zone reaches 8‰, and unweathered fine-grained materials are delivered downstream to continue weathering.

4.2 Seasonal Variations in Chemical Weathering in the Tao He, Huang Shui, and Datong He

In addition to seasonal variations in temperature, runoff is also a major factor controlling seasonal variations in chemical weathering (White and Blum, 1995). The CO_2 consumption

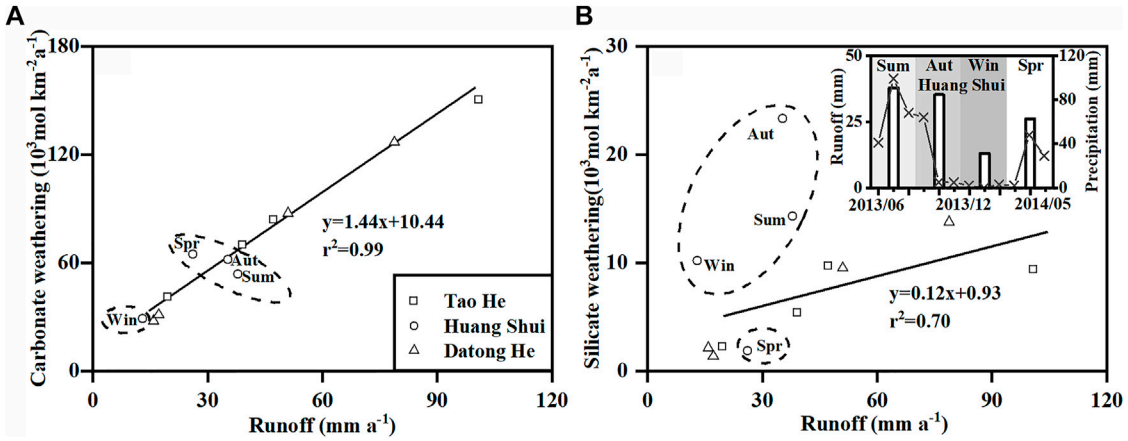

FIGURE 7 | Relationships between the CO_2 consumption rates of **(A)** carbonate and **(B)** silicate weathering and specific runoff (water discharge/surface area) at the outlets of the Tao He, Huang Shui, and Datong He throughout the year. Huang Shui data were excluded when calculating the correlation. The inset in panel B shows seasonal variations in runoff at the outlet and precipitation at the Xining station in the transition zone of the Huang Shui. The bars indicate runoff at the outlet. The black dotted line indicates the precipitation at the Xining station during the sampling period (Qinghai Water Resources Bulletin[3]). Runoff data are in **Supplementary Table S5**.

rates of carbonate weathering at the Tao He and Datong He outlets have a strong positive correlation with specific runoff (**Figure 7A**, $p < 0.05$, $r^2 = 0.99$, $n = 8$). However, for the Huang Shui, the CO_2 consumption rates of carbonate weathering in spring, summer, and autumn were not correlated with runoff. Especially in summer and autumn, the CO_2 consumption rates of carbonate weathering decreased compared to that in spring, when runoff increased. We noted that the TSS at the Huang Shui outlet in summer and autumn was about four times higher than in spring (**Table 2**). The sediment content in the Huang Shui mainly comes from the transition zone between the QTP and the LP, and the TSS at the Xining station in summer was observed to approach 9,950 mg L^{-1} (**Table 1**). Chemical weathering is limited by excessive physical erosion (Gabet and Mudd, 2009).

The relationships between the CO_2 consumption rates of silicate weathering and specific runoff for the three rivers are shown in **Figure 7B**. For the Tao He and the Datong He, the CO_2 consumption rates of silicate weathering are positively correlated with specific runoff (**Figure 7B**, $p < 0.05$, $r^2 = 0.70$, $n = 8$). However, the correlation is slightly weaker compared with the correlation between CO_2 consumption rates of carbonate weathering and specific runoff (**Figure 7A**). The main reason is that the CO_2 consumption rates of silicate weathering of the Tao He does not increase with significantly increased runoff in summer (the symbol with maximum runoff in **Figure 7B**). This may be attributed to the low CO_2 consumption rate of silicate weathering in the transition zone of the Tao He (discussed in **Section 4.1**). The CO_2 consumption rates of silicate weathering in the Huang Shui have no apparent correlation with runoff. For example, the discharge of the Huang Shui is nearly the same in summer and autumn, but the CO_2 consumption rate of silicate weathering in autumn is about twice that in summer (**Table 4**). This significant difference in the silicate weathering under similar discharges may be related to differences in the recharge sources of the river water. By comparing the seasonal variations in precipitation at the Xining station in the transition zone to the runoff at the outlet of the Huang Shui (inset in **Figure 7B**), it was found that during the sampling period, the variation of precipitation and runoff during the summer are synchronized, and both have high values. Precipitation is infrequent in autumn, whereas the runoff remains at a high level. This indicates that the river water recharge from groundwater is much greater during autumn than during summer. Groundwater contains high concentrations of silicate weathering products (Evens et al., 2004), thus exhibiting a higher calculated CO_2 consumption rate of silicate weathering in autumn than in summer. The variation in CO_2 consumption rates of silicate weathering in winter and spring are similar to those in autumn and summer, respectively, influenced by groundwater recharge.

4.3 Comparison of the CO_2 Consumption Rates by Chemical Weathering in the Tao He, Huang Shui, and Datong He With Those of Other Basins

To evaluate the CO_2 consumption rates by chemical weathering of the three rivers on the QTP, we compared the CO_2 consumption rates by chemical weathering of the three rivers with those of the other major rivers on the QTP and in other basins (**Figure 8**). The CO_2 consumption rates of silicate weathering of most rivers from the QTP are higher than the average value for the world's rivers (**Figure 8A**). In particular, values for the Ganges, Brahmaputra, and four others rivers on the southern QTP are over two times higher than the average value for the world's rivers. In contrast, the CO_2 consumption rates of silicate weathering in the Yellow River and the Indus, as well as the Tao He, Huang Shui, and Datong He on the northern QTP are significantly lower than the average value for the world's rivers.

The terrain of the QTP is high in the northwest and low in the southeast. The annual average temperature increases from −6°C

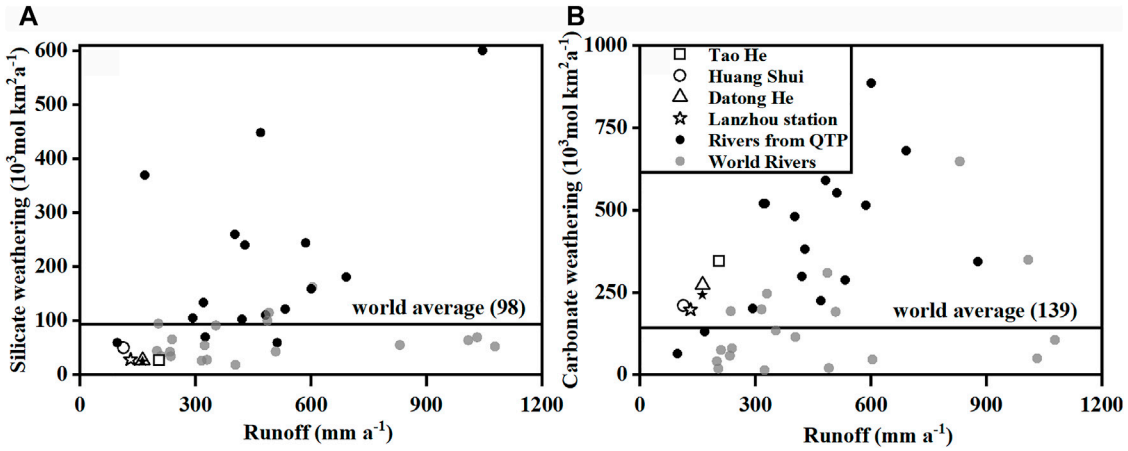

FIGURE 8 | Comparison of the CO_2 consumption rates by chemical weathering for the rivers originating on the QTP and in other basins. The unfilled symbols are the data in this paper. The black solid symbols represent data for the QTP rivers, which are from Gaillardet et al. (1999), Singh et al. (2005), Wu et al. (2008a, b), Noh et al. (2009), Wang et al. (2016), and Zhang et al. (2019). The gray solid symbols represent rivers in other basins with discharges exceeding 200 km^{3}a^{-1} (data from Gaillardet et al., 1999). The average value of CO_2 consumption rate of silicate and carbonate weathering for the world's rivers is from Gaillardet et al. (1999).

in the northwest to approximately 20°C in the southeast. The northern QTP is dominated by alpine arid and semi-arid climates, which gradually changes to a temperate semi-humid climate and finally to a humid climate toward the south. The eastern Himalayas and the Hengduan Mountains on the southern QTP have developed deep faults and extrusions that become more apparent southward. To the southern margin of the QTP, the range-gorge elevation difference reaches 1,000–1,500 m, with frequent geological activity and a highly tattered landform. Furthermore, this area is influenced by warm moist air flowing from the Indian Ocean and the Pacific Ocean. The rapid tectonic uplift and warm humid climate are likely the main reasons for the more intense silicate weathering in the southern QTP than in the northern QTP. For example, the eastern syntaxis of the Himalayas in the Brahmaputra Basin exhibits some of the highest rates of mountain uplift. The intense physical erosion and high precipitation in this area generate high CO_2 consumption rates of silicate weathering, which is comparable to the most rapidly eroding basaltic terrains such as the Reunion and Iceland (Singh et al., 2005; Hren et al., 2007). Thus, it seems that the contribution of silicate weathering to net global CO_2 uptake on the QTP may mainly come from the southern part.

As shown in **Figure 8B**, there is no significant north-south regional difference in CO_2 consumption rates of carbonate weathering of the QTP rivers. The CO_2 consumption rates of carbonate weathering fundamentally increase with increasing runoff. Furthermore, the CO_2 consumption rates of carbonate weathering of the QTP rivers are significantly higher than those of rivers with similar runoff values. However, the Indus has the lowest CO_2 consumption rate of carbonate weathering among the QTP rivers due to its low runoff, and is also much lower than the average value for the world's rivers.

In this study, a forward model is used to estimate the ion sources and CO_2 consumption by chemical weathering of the Tao He, Huang Shui, and Datong He. However, the simplification of some calculations may have introduced uncertainties into the results. For example, we uniformly calibrated the atmospheric inputs for the entire basin using the rainwater ion concentration of the QTP section. However, the three rivers straddle the QTP and the LP, and multiple climates coexist in this region, resulting in slight deviations in the estimated atmospheric inputs. Previous study shows atmospheric dust on the QTP composes ~70% of material from local sources (Zhang et al., 2001). Wu et al. (2008a) used a forward model to estimate the ions from chemical weathering of seven rivers originating from the QTP, assuming that the dust input must be local origin (i.e., redistribution of material, and thus ignoring the effect of dust input on the ion composition of river water). Due to the lack of data, it was also not considered in this study. However, ignoring dust input may result in slightly overestimated estimates of chemical weathering. Similarly, we obtained the contributions of Ca^{2+}_{sil} and Mg^{2+}_{sil} derived from silicates in the river water from the $(Ca^{2+}/Na^{+})_{sil}$ and $(Mg^{2+}/K^{+})_{sil}$ ratio of silicate fraction in the riverbed sand in the Yellow River QTP sub-basin. Although the LP section area, which has a different lithological distribution, is small, it still causes deviations in the results. Moreover, the $(Ca^{2+}/Na^{+})_{sil}$ and $(Mg^{2+}/K^{+})_{sil}$ ratio have ±50% uncertainty. Secondly, there is inaccuracy by deducting the SO_4^{2-} originating from pyrite oxidation in river water for all seasons using the percentage contribution of pyrite oxidation to SO_4^{2-} in summer at the outlets of each river. The contribution of pyrite oxidation to SO_4^{2-} varies slightly in different seasons. In addition, when we estimated the CO_2 consumption by chemical weathering based on the current concentration of major ions in the river, we did not deduct the effect of groundwater input, nor did we consider the influence of CO_2 generated form organic matter degradation and organic carbon degradation in shale. Consequently, the calculation results must be higher than the actual amount of atmospheric CO_2 absorbed by chemical weathering. All these issues need to be studied further.

5 CONCLUSION

The dissolved cations in the Tao He and Datong He are mainly from carbonate weathering, while those of the Huang Shui is dominated by evaporite dissolution. Carbonate weathering is the main contributor to the CO_2 consumption by chemical weathering in the basin. The CO_2 consumption fluxes of carbonate weathering for the Tao He, Huang Shui, and Datong He are 86.16×10^8 mol a^{-1}, 32.01×10^8 mol a^{-1} and 41.14×10^8 mol a^{-1}, respectively. The CO_2 consumption fluxes of silicate weathering are 6.65×10^8 mol a^{-1}, 7.59×10^8 mol a^{-1} and 4.02×10^8 mol a^{-1}, respectively. Although the total area of the three rivers accounts for 25% of the Yellow River QTP sub-basin, their contribution to the total CO_2 consumption flux by chemical weathering is close to 36%, with more than half of the contribution from the Tao He.

Runoff and physical erosion are the main controls on the chemical weathering of the three rivers. In addition, the increase of relief ratio in the transition zone between the QTP and the LP makes chemical weathering particularly intense in this area. The total CO_2 consumption rates by chemical weathering in the Tao He and Huang Shui transition zones are 1.4 times and 1.7 times greater than in their QTP sections, and 1.5 times and 2.0 times greater than in their LP sections, respectively. In contrast, due to the high relief ratio of 8‰ in the Datong He transition zone, the residence time of the water is extremely short, resulting in unweathered fine-grained materials being delivered downstream to continue weathering. The influence of the differential distribution of lithology on chemical weathering is mainly reflected in two aspects. Firstly, the Datong He QTP section has the highest CO_2 consumption rate of carbonate weathering in the basin due to carbonate exposure. Secondly, the low CO_2 consumption rate of silicate weathering in the transition zone of the Tao He may relate to the distribution of highly leached early Permian strata that no longer produce high chemical yields. Groundwater recharge in the Huang Shui probably has a significant effect on silicate weathering. For example, the highest calculated CO_2 consumption rate of silicate weathering occurs in autumn when groundwater recharge is highest.

In comparing rivers on the QTP with other regions of the world, the CO_2 consumption rates of silicate weathering in the Tao He, Huang Shui, Datong He, and other rivers on the northern QTP rivers are generally lower than the average value of the world's rivers and are significantly lower than those in the rivers on the southern QTP. However, the CO_2 consumption rates of carbonate weathering in QTP rivers do not exhibit regional differences from north to south. Therefore, the contribution of silicate weathering to net global CO_2 uptake on the QTP may mainly come from the southern QTP.

DATA AVAILABILITY STATEMENT

The original contributions presented in the study are included in the article/**Supplementary Material**, further inquiries can be directed to the corresponding author.

AUTHOR CONTRIBUTIONS

ZY, LZ (2nd author), and YL contributed to field investigation and sample analysis. ZY, LZ (2nd author), and LZ (4th author) contributed to the conception and data interpretation of this study and writing the manuscript. All authors contributed to manuscript revision, read, and approved the submitted version.

FUNDING

This work was supported by the National Science Foundation of China Shandong Joint Fund for Marine Science Research Centers (NSFC) (Grant No. U1606404), the Science Fund for Creative Research Groups (Grant No. 41521064), and the Science and Technology Innovation Project of High Education Institutions in Shanxi Province (Grant No. 2020L0151).

ACKNOWLEDGMENTS

We are grateful to J Wang, XB Gong and XF Yang for their help with field investigation. Thanks to QQ Jiang, CC Sui for laboratory assistance and XF Yang for providing constructive comments. We thank the editor AH, reviewer PW, and PvS for their insightful and constructive comments, which greatly improved the research content of the manuscript.

SUPPLEMENTARY MATERIAL

The Supplementary Material for this article can be found online at: https://www.frontiersin.org/articles/10.3389/feart.2021.766598/full#supplementary-material

REFERENCES

Berner, R. A., Lasaga, A. C., and Garrels, R. M. (1983). The Carbonate-Silicate Geochemical Cycle and its Effect on Atmospheric Carbon Dioxide over the Past 100 Million Years. *Am. J. Sci.* 283 (283), 641–683. doi:10.2475/ajs.283.7.641

Blum, J. D., Gazis, C. A., Jacobson, A. D., and Page Chamberlain, C. (1998). Carbonate versus Silicate Weathering in the Raikhot Watershed within the High Himalayan Crystalline Series. *Geol* 26 (5), 411–414. doi:10.1130/0091-7613(1998)026<0411:cvswit>2.3.co;2

Blum, J. D. (1997). "The Effect of Late Cenozoic Glaciation and Tectonic Uplift on Silicate Weathering Rates and the Marine 87Sr/86Sr Record," in *Tectonic Uplift and Climate Change*. Editor W. F. Ruddiman (New York: Plenum Press), 259–288. doi:10.1007/978-1-4615-5935-1_11

Chen, J., Wang, F., Meybeck, M., He, D., Xia, X., and Zhang, L. (2005). Spatial and Temporal Analysis of Water Chemistry Records (1958-2000) in the Huanghe (Yellow River) Basin. *Glob. Biogeochem. Cycles* 19 (3), 1–24. doi:10.1029/2004gb002325

Chetelat, B., Liu, C.-Q., Zhao, Z. Q., Wang, Q. L., Li, S. L., Li, J., et al. (2008). Geochemistry of the Dissolved Load of the Changjiang Basin Rivers:

Anthropogenic Impacts and Chemical Weathering. *Geochimica et Cosmochimica Acta* 72 (17), 4254–4277. doi:10.1016/j.gca.2008.06.013

Dellinger, R. W., Liu-Smith, F., and Meyskens, F. L. (2014). Continuing to Illuminate the Mechanisms Underlying UV-Mediated Melanomagenesis. *J. Photochem. Photobiol. B: Biol.* 138, 317–323. doi:10.1016/j.jphotobiol.2014.06.006

Dickson, A. G., and Goyet, C. (1994). Handbook of Methods for the Analysis of the Various Parameters of the Carbon Dioxide System in Sea Water. Version 2. *Seawater*, 1–187. doi:10.2172/10107773

Evans, M. J., Derry, L. A., and France-lanord, C. (2004). Geothermal Fluxes of Alkalinity in the Narayani River System of central Nepal. *Geochem. Geophys. Geosyst.* 5 (8), 1–21. doi:10.1029/2004GC000719

Fan, B.-L., Zhao, Z.-Q., Tao, F.-X., Liu, B.-J., Tao, Z.-H., Gao, S., et al. (2014). Characteristics of Carbonate, Evaporite and Silicate Weathering in Huanghe River Basin: A Comparison Among the Upstream, Midstream and Downstream. *J. Asian Earth Sci.* 96, 17–26. doi:10.1016/j.jseaes.2014.09.005

Gabet, E. J., and Mudd, S. M. (2009). A Theoretical Model Coupling Chemical Weathering Rates with Denudation Rates. *Geology* 37 (2), 151–154. doi:10.1130/G25270A.1

Gabet, E. J., Wolff-Boenisch, D., Langner, H., Burbank, D. W., and Putkonen, J. (2010). Geomorphic and Climatic Controls on Chemical Weathering in the High Himalayas of Nepal. *Geomorphology* 122 (1-2), 205–210. doi:10.1016/j.geomorph.2010.06.016

Gaillardet, J., Dupré, B., Louvat, P., and Allègre, C. J. (1999). Global Silicate Weathering and CO_2 Consumption Rates Deduced from the Chemistry of Large Rivers. *Chem. Geol.* 159 (1-4), 3–30. doi:10.1016/s0009-2541(99)00031-5

Galy, A., and France-lanord, C. (1999). Weathering Processes in the Ganges-Brahmaputra Basin and the Riverine Alkalinity Budget. *Chem. Geol.* 159 (1-4), 31–60. doi:10.1016/S0009-2541(99)00033-9

Gupta, H., Chakrapani, G. J., Selvaraj, K., and Kao, S.-J. (2011). The Fluvial Geochemistry, Contributions of Silicate, Carbonate and saline-alkaline Components to Chemical Weathering Flux and Controlling Parameters: Narmada River (Deccan Traps), India. *Geochimica et Cosmochimica Acta* 75 (3), 800–824. doi:10.1016/j.gca.2010.11.010

Han, G., and Liu, C.-Q. (2004). Water Geochemistry Controlled by Carbonate Dissolution: A Study of the River Waters Draining Karst-Dominated Terrain, Guizhou Province, China. *Chem. Geology.* 204 (1-2), 1–21. doi:10.1016/j.chemgeo.2003.09.009

Hartmann, J., Jansen, N., Dürr, H. H., Kempe, S., and Köhler, P. (2009). Global CO2-consumption by Chemical Weathering: What Is the Contribution of Highly Active Weathering Regions? *Glob. Planet. Change* 69 (4), 185–194. doi:10.1016/j.gloplacha.2009.07.007

Hren, M. T., Chamberlain, C. P., Hilley, G. E., Blisniuk, P. M., and Bookhagen, B. (2007). Major Ion Chemistry of the Yarlung Tsangpo-Brahmaputra River: Chemical Weathering, Erosion, and CO2 Consumption in the Southern Tibetan Plateau and Eastern Syntaxis of the Himalaya. *Geochimica et Cosmochimica Acta* 71 (12), 2907–2935. doi:10.1016/j.gca.2007.03.021

Jiang, H., Liu, W., Xu, Z., Zhou, X., Zheng, Z., Zhao, T., et al. (2018). Chemical Weathering of Small Catchments on the Southeastern Tibetan Plateau I: Water Sources, Solute Sources and Weathering Rates. *Chem. Geology.* 500, 159–174. doi:10.1016/j.chemgeo.2018.09.030

Kump, L. R., Brantley, S. L., and Arthur, M. A. (2000). Chemical Weathering, Atmospheric CO2, and Climate. *Annu. Rev. Earth Planet. Sci.* 28, 611–667. doi:10.1146/annurev.earth.28.1.611

Li, S.-L., Chetelat, B., Yue, F., Zhao, Z., and Liu, C.-Q. (2014). Chemical Weathering Processes in the Yalong River Draining the Eastern Tibetan Plateau, China. *J. Asian Earth Sci.* 88, 74–84. doi:10.1016/j.jseaes.2014.03.011

Li, S., Xia, X., Zhou, B., Zhang, S., Zhang, L., and Mou, X. (2018). Chemical Balance of the Yellow River Source Region, the Northeastern Qinghai-Tibetan Plateau: Insights about Critical Zone Reactivity. *Appl. Geochem.* 90, 1–12. doi:10.1016/j.apgeochem.2017.12.016

Meybeck, M. (1987). Global Chemical Weathering of Surficial Rocks Estimated from River Dissolved Loads. *Am. J. Sci.* 287 (5), 401–428. doi:10.2475/ajs.287.5.401

Moquet, J.-S., Crave, A., Viers, J., Seyler, P., Armijos, E., Bourrel, L., et al. (2011). Chemical Weathering and Atmospheric/soil CO2 Uptake in the Andean and Foreland Amazon Basins. *Chem. Geology.* 287 (1-2), 1–26. doi:10.1016/j.chemgeo.2011.01.005

Noh, H., Huh, Y., Qin, J., and Ellis, A. (2009). Chemical Weathering in the Three Rivers Region of Eastern Tibet. *Geochimica et Cosmochimica Acta* 73 (7), 1857–1877. doi:10.1016/j.gca.2009.01.005

Oh, N.-H., and Raymond, P. A. (2006). Contribution of Agricultural Liming to Riverine Bicarbonate export and CO2sequestration in the Ohio River basin. *Glob. Biogeochem. Cycles* 20 (3), a–n. doi:10.1029/2005GB002565

Pang, H., Pan, B., Garzanti, E., Gao, H., Zhao, X., and Chen, D. (2018). Mineralogy and Geochemistry of Modern Yellow River Sediments: Implications for Weathering and Provenance. *Chem. Geology.* 488, 76–86. doi:10.1016/j.chemgeo.2018.04.010

Raymo, M. E., and Ruddiman, W. F. (1992). Tectonic Forcing of Late Cenozoic Climate. *Nature* 359 (6391), 117–122. doi:10.1038/359117a0

Shichao, F., Xiaohong, G., Juan, G., Jian, K., Lifeng, G., Guoliang, W., et al. (2013). Land Use Spatial Distribution Modeling Based on CLUE-S Model in the Huangshui River Basin. *Acta Eco Sin* 33 (3), 985–997. doi:10.5846/stxb201204280616

Singh, S. K., Sarin, M. M., and France-Lanord, C. (2005). Chemical Erosion in the Eastern Himalaya: Major Ion Composition of the Brahmaputra and δ13C of Dissolved Inorganic Carbon. *Geochimica et Cosmochimica Acta* 69 (14), 3573–3588. doi:10.1016/j.gca.2005.02.033

Spence, J., and Telmer, K. (2005). The Role of Sulfur in Chemical Weathering and Atmospheric CO2 Fluxes: Evidence from Major Ions, δ13CDIC, and δ34SSO4 in Rivers of the Canadian Cordillera. *Geochimica et Cosmochimica Acta* 69 (23), 5441–5458. doi:10.1016/j.gca.2005.07.011

Tan, H., Zhang, W., Chen, J., Jiang, S., and Kong, N. (2012). Isotope and Geochemical Study for Geothermal Assessment of the Xining Basin of the Northeastern Tibetan Plateau. *Geothermics* 42, 47–55. doi:10.1016/j.geothermics.2012.01.001

Tang, J., Xue, H., Yu, X., Cheng, H., Xu, X., Zhang, X., et al. (2000). The Preliminary Study on Chemical Characteristics of Precipitation at Mt. Waliguan (In Chinese with English Abstract). *Acta Sci. Circumstantiae* 20 (4), 420–425.

Torres, M. A., West, A. J., and Li, G. (2014). Sulphide Oxidation and Carbonate Dissolution as a Source of CO2 over Geological Timescales. *Nature* 507 (7492), 346–349. doi:10.1038/nature13030

Wang, H., Yang, Z., Saito, Y., Liu, J. P., and Sun, X. (2006). Interannual and Seasonal Variation of the Huanghe (Yellow River) Water Discharge over the Past 50 years: Connections to Impacts from ENSO Events and Dams. *Glob. Planet. Change* 50 (3-4), 212–225. doi:10.1016/j.gloplacha.2006.01.005

Wang, J., and Hu, X. (2011). Runoff Space-Time Distribution Rule and Evolution Tendency of Yellow River Upstream and Main Tributaries (In Chinese with English Abstract). *J. Chin. Hydrol.* 31 (3), 90–96.

Wang, L., Huang, W., Shi, Z., and Kang, F. (2012). Spatial and Temporal Characteristics of Runoff in Datong River basin. Gans. Water (In Chinese). *Resour. Hydropow. Technol.* 48 (8), 1–14.

Wang, L., Zhang, L., Cai, W.-J., Wang, B., and Yu, Z. (2016). Consumption of Atmospheric CO2 via Chemical Weathering in the Yellow River basin: The Qinghai-Tibet Plateau Is the Main Contributor to the High Dissolved Inorganic Carbon in the Yellow River. *Chem. Geology.* 430, 34–44. doi:10.1016/j.chemgeo.2016.03.018

Wang, Y., and Chen, J. (1897). *Metamorphic Sequences and Metamorphism of Qinghai Province and Surrounding Areas (In Chinese)*. Beijing, CHN: Geological Publishing House.

West, A., Galy, A., and Bickle, M. (2005). Tectonic and Climatic Controls on Silicate Weathering. *Earth Planet. Sci. Lett.* 235 (1-2), 211–228. doi:10.1016/j.epsl.2005.03.020

West, J. A., Bickle, M. J., Collins, R., and Brasington, J. (2002). Small-catchment Perspective on Himalayan Weathering Fluxes. *Geol* 30 (4), 355–358. doi:10.1130/0091-7613(2002)030<0355:scpohw>2.0.co;2

White, A. F., and Blum, A. E. (1995). Effects of Climate on Chemical_ Weathering in Watersheds. *Geochimica et Cosmochimica Acta* 59 (9), 1729–1747. doi:10.1016/0016-7037(95)00078-E

Wu, L., Huh, Y., Qin, J., Du, G., and van der Lee, S. (2005). Chemical Weathering in the Upper Huang He (Yellow River) Draining the Eastern Qinghai-Tibet Plateau. *Geochimica et Cosmochimica Acta* 69 (22), 5279–5294. doi:10.1016/j.gca.2005.07.001

Wu, W. (2016). Hydrochemistry of Inland Rivers in the North Tibetan Plateau: Constraints and Weathering Rate Estimation. *Sci. Total Environ.* 541, 468–482. doi:10.1016/j.scitotenv.2015.09.056

Wu, W., Xu, S., Yang, J., and Yin, H. (2008a). Silicate Weathering and CO2 Consumption Deduced from the Seven Chinese Rivers Originating in the Qinghai-Tibet Plateau. *Chem. Geology.* 249 (3-4), 307–320. doi:10.1016/j.chemgeo.2008.01.025

Wu, W., Yang, J., Xu, S., and Yin, H. (2008b). Geochemistry of the Headwaters of the Yangtze River, Tongtian He and Jinsha Jiang: Silicate Weathering and CO2 Consumption. *Appl. Geochem.* 23 (12), 3712–3727. doi:10.1016/j.apgeochem.2008.09.005

Yang, D., Li, C., Hu, H., Lei, Z., Yang, S., Kusuda, T., et al. (2004). Analysis of Water Resources Variability in the Yellow River of China during the Last Half century Using Historical Data. *Water Resour. Res.* 40, 1–12. doi:10.1029/2003WR002763

Zhang, D., Zhao, Z.-q., Li, X.-d., Zhang, L.-l., Chen, A.-c., and Chen, A. (2020b). Assessing the Oxidative Weathering of Pyrite and its Role in Controlling Atmospheric CO2 Release in the Eastern Qinghai-Tibet Plateau. *Chem. Geology.* 543, 119605. doi:10.1016/j.chemgeo.2020.119605

Zhang, D., Zhao, Z.-Q., Peng, Y., Fan, B., Zhang, L., Li, J., et al. (2020a). Sulfur Cycling in the Yellow River and the Sulfate Flux to the Ocean. *Chem. Geology.* 534, 119451. doi:10.1016/j.chemgeo.2019.119451

Zhang, J., Huang, W., Letolle, R., and Jusserand, C. (1995). Major Element Chemistry of the Huanghe (Yellow River), China - Weathering Processes and Chemical Fluxes. *J. Hydrol.* 168 (1-4), 173–203. doi:10.1016/0022-1694(94)02635-O

Zhang, X., Xu, Z., Liu, W., Moon, S., Zhao, T., Zhou, X., et al. (2019). Hydro-Geochemical and Sr Isotope Characteristics of the Yalong River Basin, Eastern Tibetan Plateau: Implications for Chemical Weathering and Controlling Factors. *Geochem. Geophys. Geosyst.* 20 (3), 1221–1239. doi:10.1029/2018GC007769

Zhang, X. Y., Arimoto, R., Cao, J. J., An, Z. S., and Wang, D. (2001). Atmospheric Dust Aerosol over the Tibetan Plateau. *J. Geophys. Res.* 106 (D16), 18471–18476. doi:10.1029/2000JD900672

Zheng, M. (1997). *An Introduction to Saline Lakes on the Qinghai-Tibet Plateau.* Dordrecht: Kluwer Acadamic Publisher.

Zhou, M.-F., Robinson, P. T., Wang, C. Y., Zhao, J.-H., Yan, D.-P., Gao, J.-F., et al. (2012). Heterogeneous Mantle Source and Magma Differentiation of Quaternary Arc-like Volcanic Rocks from Tengchong, SE Margin of the Tibetan Plateau. *Contrib. Mineral. Petrol.* 163 (5), 841–860. doi:10.1007/s00410-011-0702-8

Zhu, J., Zhang, Y., Tang, Y., and Duan, Z. (2012). Analysis of Characteristics of Runoff Variation in Taohe River Mainsteam (In Chinese). *Yellow River* 34 (1), 27–30.

Conflict of Interest: The authors declare that the research was conducted in the absence of any commercial or financial relationships that could be construed as a potential conflict of interest.

Publisher's Note: All claims expressed in this article are solely those of the authors and do not necessarily represent those of their affiliated organizations, or those of the publisher, the editors and the reviewers. Any product that may be evaluated in this article, or claim that may be made by its manufacturer, is not guaranteed or endorsed by the publisher.